Available online at www.sciencedirect.com
SCIENCE DIRECT®
Polymer 45 (2004) 2793–2802
polymer
www.elsevier.com/locate/polymer

Structure-property relationships of in-situ PMMA modified nano-sized antimony trioxide filled poly(vinyl chloride) nanocomposites

Xiao-Lin Xie[a,b,*], Robert Kwok-Yiu Li[c], Qing-Xi Liu[a,c], Yiu-Wing Mai[b]

[a]*Department of Chemistry, Huazhong University of Science and Technology, Wuhan 430074, China*
[b]*Center for Advanced Materials Technology (CAMT), School of Aerospace, Mechanical and Mechatronic Engineering (J07), The University of Sydney, Sydney, NSW 2006, Australia*
[c]*Department of Physics and Materials Science, City University of Hong Kong, Hong Kong, HKSAR, China*

Received 4 November 2003; received in revised form 7 February 2004; accepted 17 February 2004

Abstract

Nano-sized antimony trioxide (Sb_2O_3) particles were modified by in-situ methyl methacrylate (MMA)/Sb_2O_3 polymerization. Subsequently, these modified nanoparticles were compounded with poly(vinyl chloride) (PVC) to prepare PVC/Sb_2O_3 nanocomposites. In-situ MMA/Sb_2O_3 polymerization kinetics shows that nano-Sb_2O_3 particles do not inhibit polymerization of MMA. PMMA shell covered on the surface of nano-sized Sb_2O_3 particles have enhanced interactions with PVC matrix, breaking down nano-Sb_2O_3 particle agglomerates and improving their dispersion in the matrix (average particle size of 60–80 nm) and also increasing the particle-matrix interfacial adhesion. Thus, nano-Sb_2O_3 particles reinforce and toughen PVC. It was observed that at 2.5 wt% of nano-Sb_2O_3 particles modified by in-situ PMMA optimal properties were achieved in Young's modulus, tensile yield strength, elongation at break and Charpy notched impact strength. Detailed examinations of micro-failure mechanisms of tensile specimens showed that nano-Sb_2O_3 particles acted as stress concentrators leading to debonding/voiding and deformation of the matrix material around the nanoparticles. Under impact fracture, the nano-Sb_2O_3 particles prolonged crack initiation time, and increased energy absorptions for crack initiation and fracture propagation caused by strong interfacial interaction between nanoparticles and PVC matrix. These mechanisms lead to impact toughening of the nanocomposites.

Keywords: Nanocomposites; Surface modification; In-situ polymerization

1. Introduction

Fillers have important roles in modifying the properties of various polymers and lowering the cost of their composites. The effect of fillers on properties of composites depends on their level of loading, shape and particle size, aggregate size, surface characteristics and degree of dispersion. Recently, polymer-matrix nanocomposites have attracted considerable attention owing to their unique mechanical, optical, electric and magnetic properties, and strong interactions with the matrix resulting from the nano-scale microstructure and extremely large interfacial area between filler and matrix [1–5]. It is well known that the mechanical properties of composites are strongly related to the filler aspect ratio. Thus, layered silicate, like montmorillonite, has been extensively studied in recent years due to its fairly large aspect ratio [6–8]. The polymer/intercalated or exfoliated montmorillonite nanocomposites possess high strength, superior modulus, good heat distortion temperature and superior barrier properties, but their low fracture toughness has greatly limited their applications. The challenge is to find novel methods to increase the fracture toughness [9]. In contrast, nano-sized particles, such as silica and calcium carbonate, filled-polymer composites will possess significant improvements in both rigidity and toughness if the ultra-fine phase dimensions of the nanoparticles are maintained after compounding with a given polymer matrix [9–19].

The homogeneous dispersion of nanoparticles in polymer matrix is very difficult because they have a strong tendency to agglomerate. The sol–gel process provides a method of preparation of inorganic metal oxides under mild conditions

* Corresponding author. Address: Department of Chemistry, Huazhong University of Science and Technology, Wuhan 430074, China. Tel.: +86-27-87544831; fax: +86-27-87543632.
E-mail address: xiaolin.xie@aeromech.usyd.edu.au (X.L. Xie).

0032-3861/$ - see front matter © 2004 Elsevier Ltd. All rights reserved.
doi:10.1016/j.polymer.2004.02.028

starting from organic metal alkoxides [20–24] and allows structural variation without compositional alteration. But the formation of a crosslinked network of organic metal oxides makes it difficult to process, which is a disadvantage that circumscribes the application of this method [11]. In-situ polymerization is commonly used to prepare nanoparticle-filled composites with good dispersion, where the nanoparticles are first dispersed in the monomer; then, the mixture is polymerized using a technique similar to bulk polymerization [10,11,25]. However, the method is not suitable for polyolefin-matrix nanocomposites because of the low catalytic activity of the Ziegler–Natta catalyst supported on the surface of nano-filler and low conversion of monomer [26]. It is well accepted that the widely used compounding technique for preparation of conventionally filled polymers is still the most convenient way when nanoparticles are proposed to replace the micro-sized fillers for high-performance polymers [9,15]. Some efforts have been focused to modify the surface of nanoparticles to prepare homogeneously dispersed nanocomposites. Hergeth and co-workers [27–29] first applied an emulsion polymerization process to encapsulate inorganic particles by a polymer layer, so-called core-shell particles, where the in-situ polymerization of the monomer occurred mainly at the surface of unmodified particles due to the adsorption of monomer on the surface, followed by polymerization in the adsorbed layer. Then, Bourgeat-Lami et al. functionalized inorganic nanoparticles and treated the particles by in-situ emulsion polymerization [30–35]. Rong et al. modified the nano-sized silica by irradiation grafting of monomer, then compounded it with polypropylene [15,16]. Radhakrishnan and co-worker synthesized nano-sized calcium phosphate by in-situ deposition technique in the presence of poly-(ethylene oxide), then compounded it with polypropylene [18]. The in-situ polymers covered on the surface of the nanoparticles break down these nanoparticle agglomerates and enhance the dispersion of nanoparticles in the matrix. Recently, Xie et al. modified micro-sized talc and glass beads with polymerization of a particular monomer, so-called in-situ monomer/inorganic particle polymerization [36,37]. Since the polymer of the selected monomer is thermodynamically miscible with the composite matrix, the polymer shell on the particles increases the interfacial adhesion of these inorganic particles with, and also promotes particle dispersion in, the composite matrix. The same in-situ monomer/inorganic particle polymerization method can be applied to inorganic nanoparticles. In the present work, we have employed this technique to modify nano-sized antimony trioxide (Sb_2O_3) particles with a monomer, methyl methacrylate (MMA). Subsequently, these modified nanoparticles were compounded with poly(vinyl chloride) (PVC) to prepare PVC/Sb_2O_3 nanocomposites. The Sb_2O_3 nanoparticle was selected as it is expected to improve synergistically the flame retardance of PVC.

The main aim of this research was to study the effect of in-situ PMMA modified nano-Sb_2O_3 particles on the structure and properties of PVC-matrix nanocomposites. It is expected that the PMMA shell on the surface of nano-Sb_2O_3 may enhance the dispersion of nano-Sb_2O_3 in PVC and improve the interfacial bonding between the nanoparticles and the matrix.

2. Experimental work

2.1. Materials

PVC (type S3), with an average polymerization degree between 1250 and 1350, was provided by Wuhan Gedian Chemical Industry Co. Ltd, China. Nano-Sb_2O_3 powders with average primary particle size of 30–40 nm, were supplied courtesy of Wuhan Petroleum Chemical Co., China. Chemically pure grade MMA, a commercial monomer, was purified by distillation under reduced pressure before being used to remove the inhibitor. The thermal stabilizer (XP-301) was a mixture of plumb salts. The processing aid (ACR-401) was an acrylate resin. They were provided by Zibo Plastic Chemical Co., China. Paraffin wax and stearic acid were industrial grade products, and were commercially available.

2.2. Surface modification of nano-Sb_2O_3 particles by in-situ MMA/Sb_2O_3 polymerization

Surface modification of nano-Sb_2O_3 particles with 10 wt% MMA (based on nano-Sb_2O_3 particles) were carried out by in-situ MMA/nano-Sb_2O_3 polymerization at 70 °C according to conditions given in Ref. [36]. In-situ MMA/nano-Sb_2O_3 polymerization was performed by batch seed emulsion polymerization in a 5000 ml glass reactor (stirring rate 200 rpm) as follows. First, nano-Sb_2O_3 was dispersed in aqueous water ultrasonically. The ingredients (deionized water, sodium dodecyl sulfonate (SDS) as emulsifier, MMA as monomer) were added to the reactor vessel, heated and stirred continuously, until the reaction temperature was reached. Then, an aqueous solution of ammonium persulfate (APS), with an amount 1% of MMA, as initiator (and preheated to reaction temperature), was added to start the polymerization reaction. At the same time, the reaction time was recorded. Before adding the initiator the glass reactor equipped with stirrer was purged with N_2 six times. The products were spray-dried at 80 °C after emulsion breakage. Subsequently, they were dried at 60 °C under vacuum to a constant weight about 48 h.

The particle size distributions of unmodified and modified nano-Sb_2O_3 particles were determined by a COULTER LS-230 particle size tester before emulsion breakage. The products were dried at 45 °C under vacuum after emulsion breakage and centrifugation. The conversion

was determined by:

$$\text{Conversion (\%)} = \frac{\text{precipitate (g)} - \text{nanoparticles (g)}}{\text{monomer used (g)}} \times 100\% \quad (1)$$

2.3. Preparation of nano-Sb_2O_3 filled PVC nanocomposites

The composition of the PVC nanocomposite is: 100 parts PVC, 7 parts XP-301, 2 parts ACR-401, 0.6 parts paraffin wax (intermediate lubricant), and 0.8 parts stearic acid. PMMA-coated nano-Sb_2O_3 and unmodified nano-Sb_2O_3 were mixed with the PVC matrix mixture in a high-speed mixer, respectively. The composite mixtures were plasticized by a two-roll-mill at 180 °C for 10 min. Composite plates with dimensions of $200 \times 80 \times 3.2\ mm^3$ were compression-moulded at 180 °C for 8 min, with a 5-min preheating period. Care was taken at this stage to ensure precise timing so as to eliminate any difference that might arise as a result of the samples having different thermal histories. These plates were cut into dog-bone shaped tensile bars. Notched Charpy impact specimens were also prepared in a similar way except the thickness was 6 mm.

2.4. Differential scanning calorimetry (DSC)

DSC measurements were conducted in a TA Instrument DSC analyzer (model 2910) at a heating rate of 10 °C min^{-1} in dry nitrogen. Prior to testing, all samples were heated and kept at a constant temperature of 200 °C for 3 min to eliminate any influence of their previous thermal histories. Then they were quenched to ambient temperature.

2.5. Dynamic mechanical analysis (DMA)

Dynamic mechanical analysis (DMA) was conducted in a TA Instrument dynamic mechanical analyser (model 2980) at a fixed frequency of 1 Hz and an oscillation amplitude of 20 μm. The temperature range studied was from −20 to 130 °C with a heating rate of 2 °C min^{-1}.

2.6. Morphology observations

The morphologies of the fracture surfaces of all composites were observed in a scanning electron microscope (JEOL JSM 820). The specimens were coated with a thin layer of gold prior to SEM examination.

2.7. Mechanical properties

Tensile tests were performed with an Instron tensile tester (type 5567) at a crosshead speed of 1 mm min^{-1} at room temperature. Notched Charpy impact specimens were cut from the plaques with dimensions of $200 \times 80 \times 6\ mm^3$, and were tested by a Ceast Fractovis instrumented drop-weight dart impact tester. Blunt notches with a tip radius of 0.25 mm were introduced to the impact specimens with a Ceast notch opener. The impact velocity was fixed at 2 m s^{-1}. The force–time curves exhibited various noises due to force oscillations generated in the tests. Some researchers applied electronic and mechanical filters to treat these signals [38,39]. But, we used Fourier transform to filter the noise from the experimental signals [40–42].

3. Results and discussion

3.1. Reaction kinetics of in-situ MMA/nano-Sb_2O_3 polymerization

Fig. 1 shows reaction kinetics of batch in-situ MMA/nano-Sb_2O_3 polymerization at different temperatures. The weight ratio of nano-Sb_2O_3 and MMA is 1:1. The results indicate that the temperature significantly affect the polymerization rate. The higher the temperature, the earlier the auto-acceleration occurs and the shorter the time to achieve equilibrium conversion. For the three temperatures studied, the final conversions all approach 97%. Thus, it can be concluded that the nano-Sb_2O_3 does not inhibit the polymerization of MMA.

3.2. Particle size and distribution

Fig. 2 shows TEM images of unmodified Sb_2O_3 particles dispersed in ethanol. We can see that most Sb_2O_3 particles agglomerate, but the primary average particle size is 30–40 nm. Figs. 3 and 4 show the particle size distribution of pristine and modified Sb_2O_3 treated for different time. It can be seen that there are four peaks in the particle size distribution of unmodified nano-sized Sb_2O_3 particles, which are located at about 0.1, 4.2, 12.5 and 25 μm, respectively. Compared to Fig. 2, we can infer that the peaks

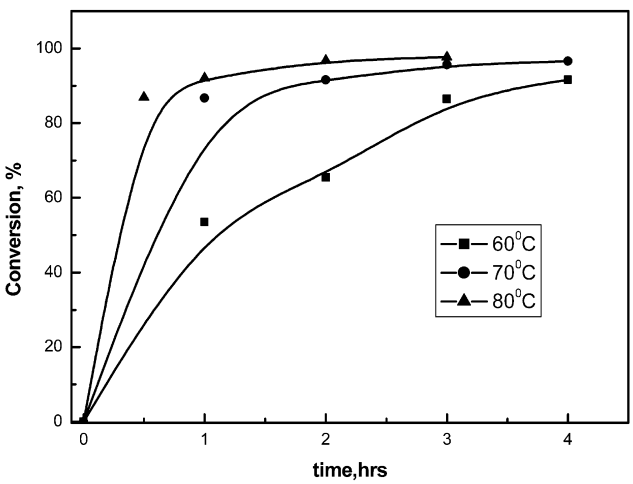

Fig. 1. Kinetics curves of Sb_2O_3/MMA in-situ polymerization.

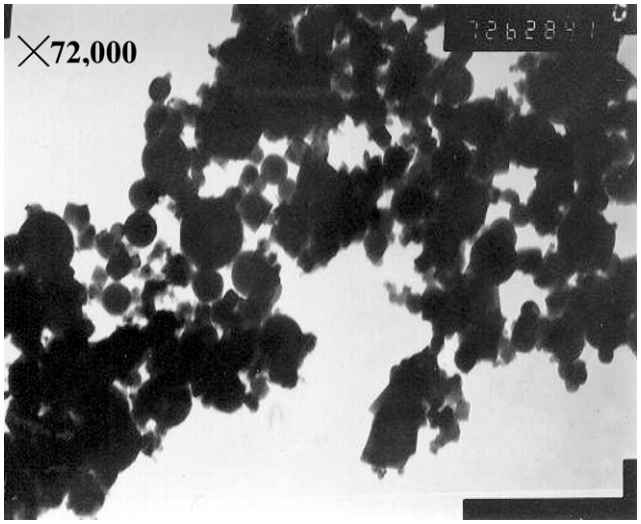

Fig. 2. TEM micrograph of Sb_2O_3 particles. (× 72,000).

located at 4.2, 12.5 and 25 μm are the aggregate peaks of nano-sized particles. When Sb_2O_3 particles were modified by in-situ MMA/nano-Sb_2O_3 polymerization for 1 h, the peaks located at 4.2, 12.5 and 25 μm disappeared, and a new peak at 2.2 μm emerged. From the TEM micrograph of Sb_2O_3 particles (see Fig. 2), there are many gaps and empty space around the particles. It is well known that such particles, owing to the weak force that stack them together, can be easily separated in a solvent. During polymerization reaction, MMA may enter the gaps and empty space between the primary particles under an ultrasonic environment. So, polymerization can be initiated by diffusion of an initiator and the heat released inside the gaps lead to breakdown of the nano-Sb_2O_3 particle agglomerates. After being modified for 4 h, the particle size distribution of nano-Sb_2O_3 particles tends to a single peak at 5.2 μm. The increasing average size of nano-sized Sb_2O_3 particles is

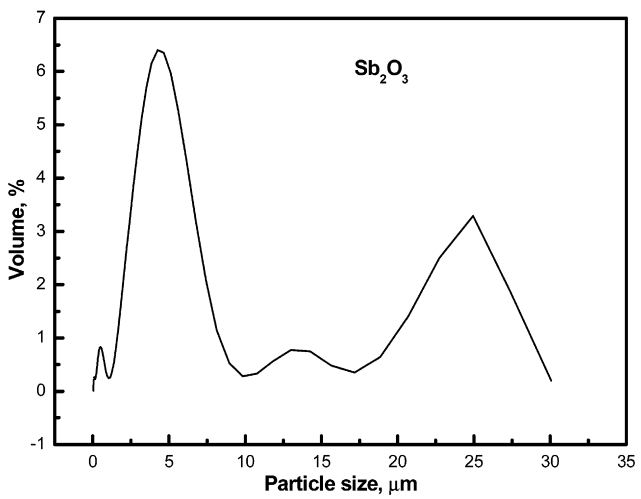

Fig. 3. Particle size distribution of untreated Sb_2O_3.

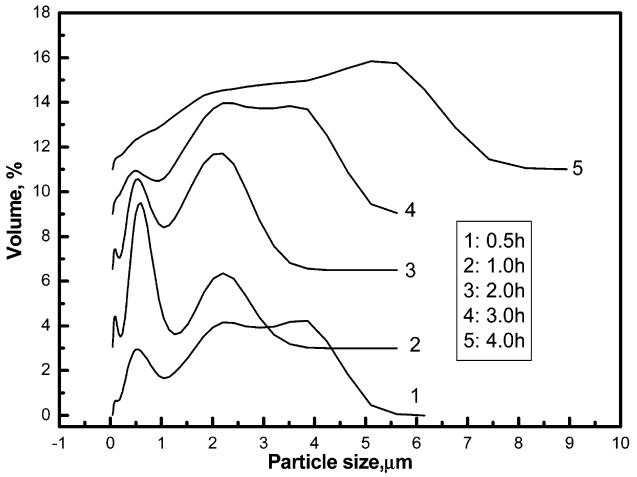

Fig. 4. Particle size distribution of treated Sb_2O_3 at different time during polymerization reaction.

related to the PMMA shell coated on the surface of nanoparticles. So we believe that PMMA shells covered on the surfaces of nano-sized Sb_2O_3 particles suppress the aggregation of nano-sized particles effectively. It should be mentioned that the size of the nanoparticles is measured before emulsion breakage, PMMA chain segments covered on the surfaces of nano-Sb_2O_3 particles are hairy in form, and the nanoparticles may be connected by PMMA chains. These factors lead to modified nano-Sb_2O_3 particles being in microns. However, when they are compounded with the polymer matrix at the molten state, they will be broken down and dispersed in the matrix in nano-meter scale.

3.3. Morphologies of nanocomposites

Dispersion of fillers in a polymer matrix has significant effects on the mechanical properties of composites [43,44]. But dispersion of inorganic fillers in thermoplastics is not an easy process. Especially, when the filler size decreases to nanometer scale, the problem will become serious because the nanoparticles have a strong tendency to self-agglomerate.

SEM micrographs of cryogenic-fractured PVC/nano-Sb_2O_3 composites are shown in Fig. 5. Nano-Sb_2O_3 particles coated by PMMA are uniformly dispersed in the PVC matrix, Fig. 5(a) and (b), with an average size of 60–80 nm for nanoparticle loading of 2.5 and 5.0 wt%. Compared to the morphology of PVC, Fig. 5(d), these micro-size domains are in fact stabilizers, such as plumb stearate, by EDAX. Moreover, we can see the good interfacial bonding between nanoparticles and PVC matrix owing to the large interfacial area of nanoparticles and compatibilization of PMMA shell on the surface of nanoparticles. With further increase of nanoparticles loading to 7.5 wt% in the composites, the modified nanoparticles tend to aggregate, Fig. 5(c).

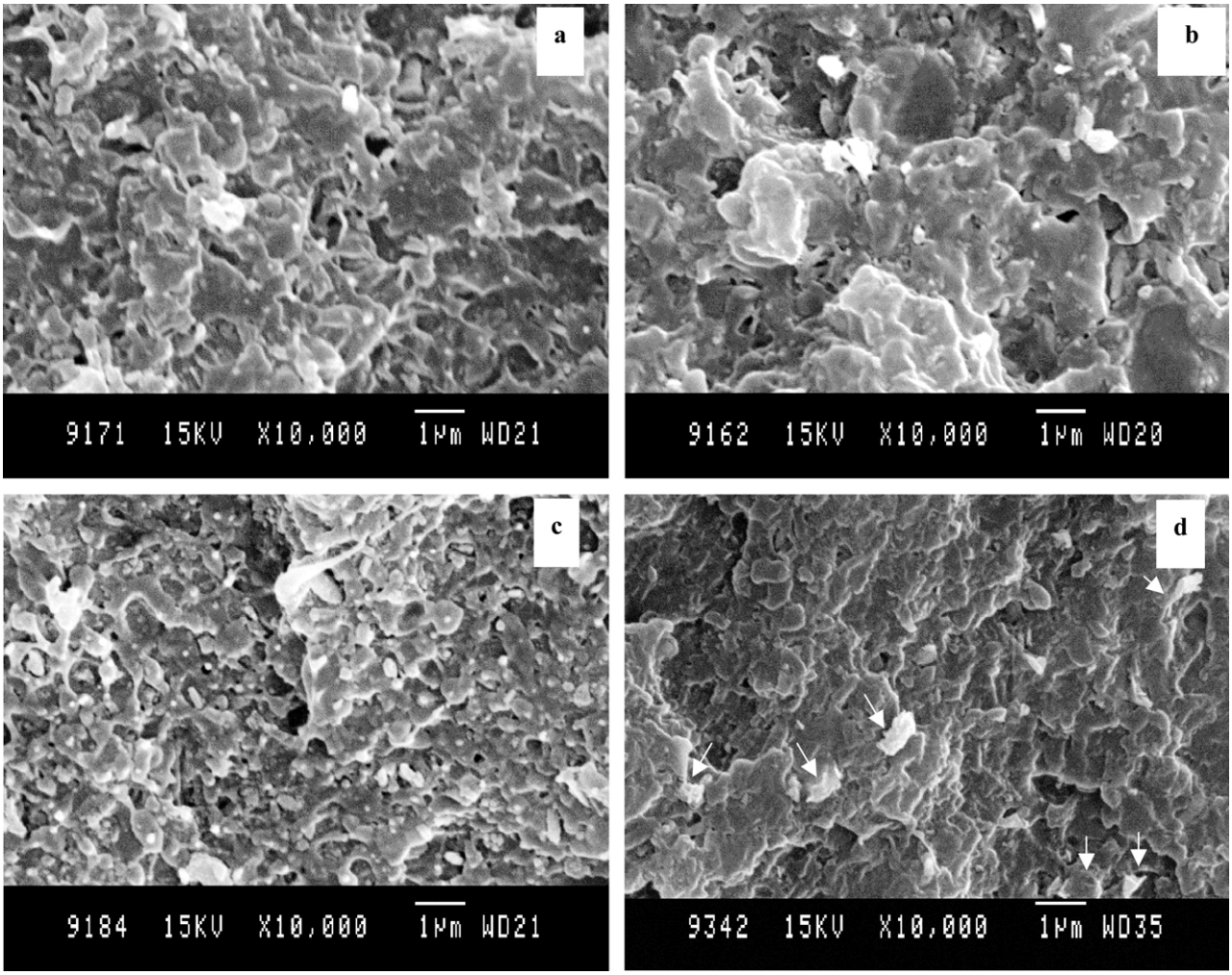

Fig. 5. SEM micrographs of cryogenic-fractured PVC and PVC/nano-Sb_2O_3 composites. (a) 2.5 wt% nano-Sb_2O_3; (b) 5.0 wt% nano-Sb_2O_3; (c) 7.5 wt% nano-Sb_2O_3; and (d) pure PVC.

3.4. Glass transition temperature of PVC matrix in nanocompoistes

Fig. 6 shows DSC heating curves for PVC and PVC/Sb_2O_3 nanocomposites. It can be seen that the glass transition temperature (T_g) of PVC increases to 73.04 °C from 69.74 °C by adding 2.5 wt% of in-situ PMMA modified nano-Sb_2O_3 particles. At 5.0 wt% of modified nanoparticles, T_g of PVC further increases to 74.33 °C. However, T_g of PVC decreases to 71.63 °C with modified nanoparticles of 7.5 wt%. DMA results, Fig. 7, also show similar behavior. Obviously, the glass transition peak of PVC in the PVC/Sb_2O_3 nanocomposites tends to shift toward higher temperature as the loading of modified nanoparticles is less than 7.5 wt%. As mentioned above, the amount of MMA is about 10% based on nano-Sb_2O_3 particles, the maximum content of PMMA in the nanocomposite is only 0.75 wt%, so the effect of PMMA on the glass transition temperature of PVC phase in the nanocomposite can be neglected. This is because PMMA is miscible with PVC thermodynamically [45] so that the PMMA shell

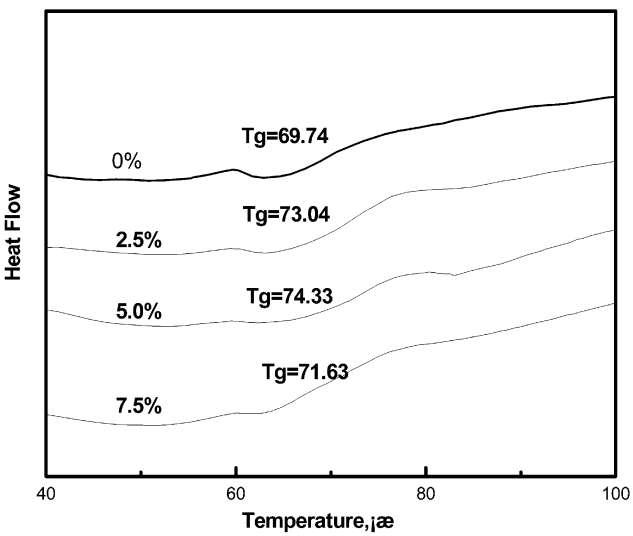

Fig. 6. DSC heating curves for PVC and PVC/Sb_2O_3 nanocomposites.

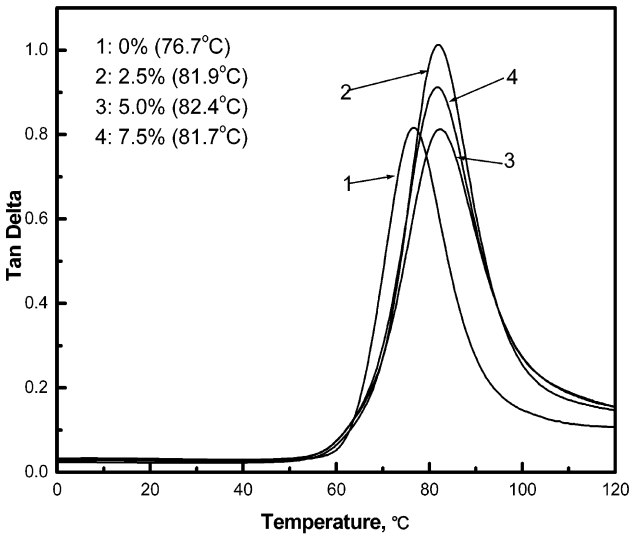

Fig. 7. Variation of tan δ with temperature for PVC and PVC/Sb_2O_3 nanocomposites.

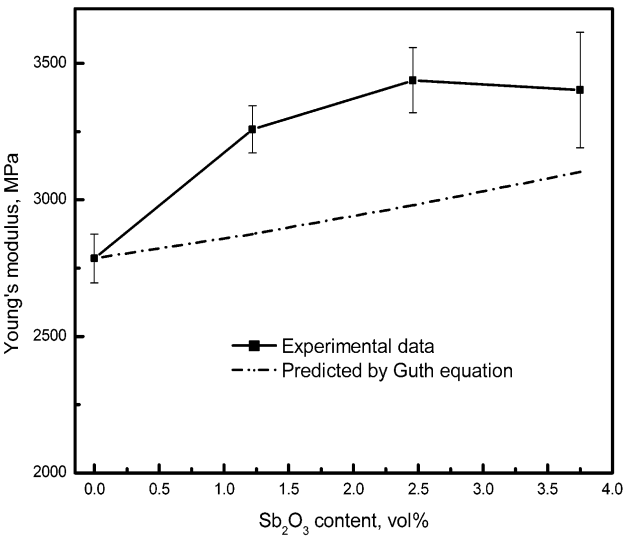

Fig. 9. Effect of nano-Sb_2O_3 particle volume fraction on Young's modulus of the nanocomposites.

on nano-Sb_2O_3 particles increases the interaction between the particles and PVC matrix. Consequently, nano-Sb_2O_3 particles restrain the thermal motion of PVC molecular chains leading to enhancement of T_g of PVC. As the nano-Sb_2O_3 particles are increased to 7.5 wt%, they agglomerate. Hence, the interaction between nano-Sb_2O_3 particles and PVC is weakened, and T_g of PVC is decreased.

3.5. Mechanical properties

Fig. 8 shows the tensile stress–displacement curves for PVC and nanocomposites. Clearly, pure PVC is brittle. When nano-Sb_2O_3 particles are added in PVC matrix, the nanocomposites show ductile behaviours, such as stress whitening and necking. Their Young's modulus, tensile yield strength and elongation at break are calculated and plotted in Figs. 9 and 10.

In Fig. 9, it is shown that Young's modulus of the PVC/Sb_2O_3 nanocomposites increases with the loading of nano-Sb_2O_3 particles to 2.5 wt% and then decreases marginally at 5.0 wt%. Similar observations are noticed for the tensile yield strength data in Fig. 10, in which a maximum is seen at 2.5 wt% nanoparticle loading followed by a gradual decrease. These results confirm that nano-Sb_2O_3 particles have both stiffening and strengthening effects on PVC. They can be compared to the predicted moduli and yield strengths of particle-filled composites, respectively, by Guth's equation [46]:

$$E_c = E_m(1 + 2.5\phi_f + 14.1\phi_f^2) \quad (2)$$

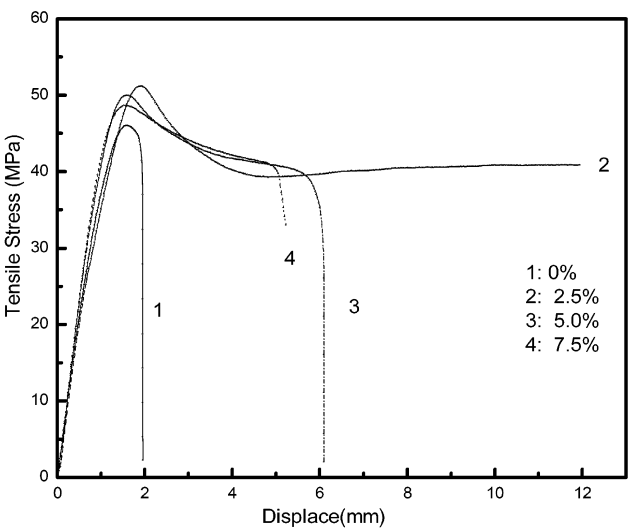

Fig. 8. Tensile stress–displacement curves for PVC and PVC/Sb_2O_3 nanocomposites.

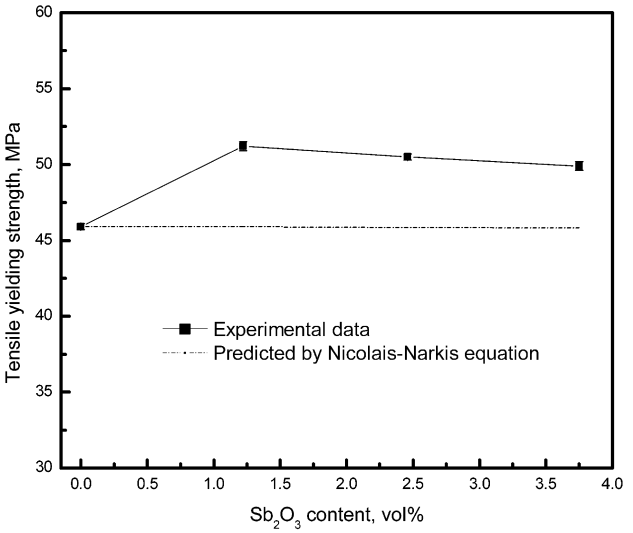

Fig. 10. Variation of tensile yield strength of nanocomposite with nanoparticle volume fraction.

and Nicolais–Narkis equation [47]:

$$\sigma_{yc} = \sigma_{ym}(1 - 1.21\phi_f^{2/3}) \quad (3)$$

where (E_c, E_m) and (σ_{yc}, σ_{ym}) are moduli and yield strengths of composite (subscript c) and matrix (subscript m), respectively, and ϕ_f is volume fraction of particles. Quite clearly, the predicted values are all lower than the experimental data as shown in Figs. 9 and 10, indicating that there is strong interaction between nano-Sb_2O_3 particles and PVC matrix due to the PMMA shell coated on the surface of the nanoparticles and the large interfacial area.

Turcsanyi et al. [48] gave a quantitative relationship between tensile strength and interfacial interaction by:

$$\sigma_{yc} = \sigma_{ym}\frac{1 - \phi_f}{1 + 2.5\phi_f}\exp(B_{\sigma y}\phi_f) \quad (4)$$

where $B_{\sigma y}$ is a measure of interfacial interaction. The larger $B_{\sigma y}$, the stronger is the interfacial interaction. To evaluate the interaction between nano-Sb_2O_3 particles and PVC matrix, $(\ln[\sigma_{yc}/\sigma_{ym}] + \ln[(1 + 2.5\phi_f)/(1 - \phi_f)])$ is plotted against ϕ_f in Fig. 11 which gives $B_{\sigma y} = 2.36$. Whilst $B_{\sigma y}$ has no direct physical meaning, it is obviously connected with the interfacial interaction of composites. For ABS polymer filled with glass beads, $B_{\sigma y} = 0.246$ was determined and approximated the 'no adhesion' case by Turcsanyi et al. [48]. For PVC/Sb_2O_3 nanocomposites, the high $B_{\sigma y}$ value indicates that the interfacial adhesion between nanoparticles and PVC matrix is very strong and tends to prevent debonding at the matrix-particle interface during tensile deformation [49]. As shown in Fig. 12, the elongation of the nanocomposite at break is higher than that of PVC, and the elongation is maximum when the loading of nanoparticles is also 2.5 wt%.

Fig. 13 plots the variation of Charpy notched impact strength of nanocomposites with nano-Sb_2O_3 particle content. When 2.5 wt% nanoparticles coated by PMMA are added to PVC, Charpy impact strength increases to 5.85 kJ m^{-2} from 3.09 kJ m^{-2} of PVC. However, further increase in nano-Sb_2O_3 particles loading causes the notched impact strength of the nanocomposite to decrease owing to the aggregation of nanoparticles in the PVC matrix. The results are consistent with the tensile modulus and strength behaviours of the nanocomposites.

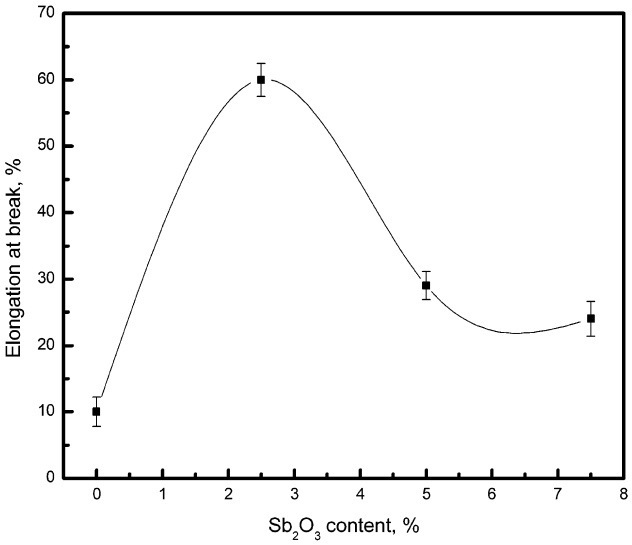

Fig. 12. Variation of elongation of nanocomposites at break with nanoparticle loading.

3.6. Fracture micro-mechanism

To study the impact behaviour of PVC/Sb_2O_3 nanocomposites, instrumented drop weight dart impact tests were

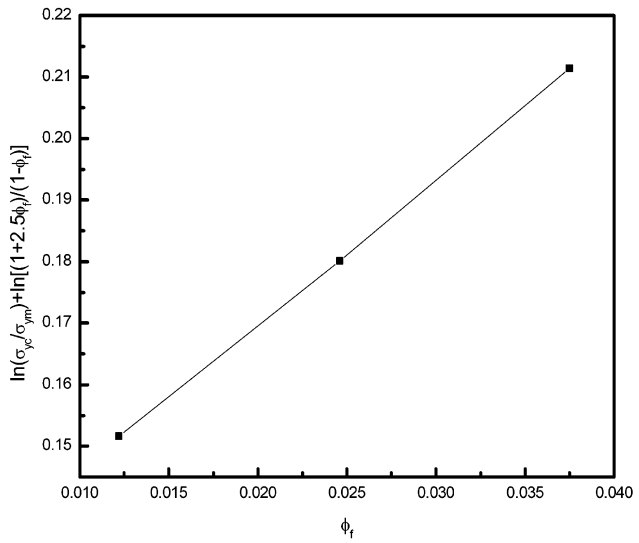

Fig. 11. Relationship between $(\ln[\sigma_{yc}/\sigma_{ym}] + \ln[(1 + 2.5\phi_f)/(1 - \phi_f)])$ and ϕ_f.

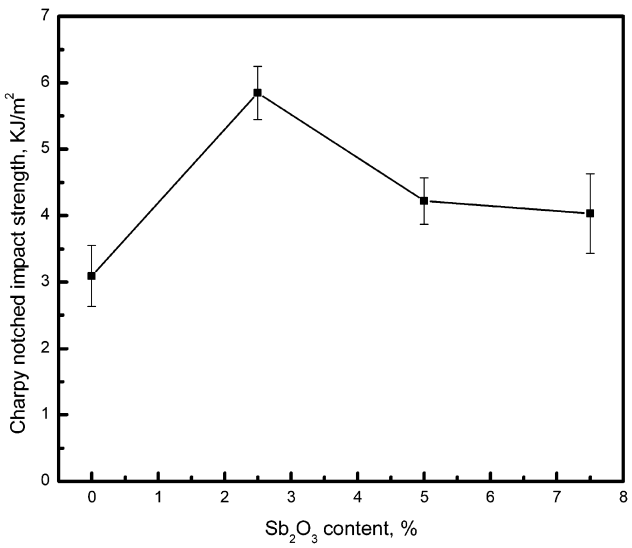

Fig. 13. Variation of Charpy notched impact strength of nanocomposites with nanoparticle loading.

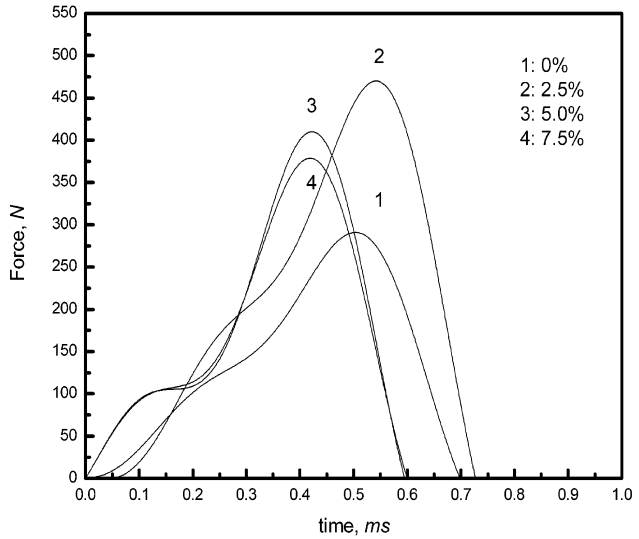

Fig. 14. Force–time curves of drop-weight dart impact test for PVC and PVC/Sb_2O_3 nanocomposites.

used to examine the fracture process. Fig. 14 shows the force–time curves filtered by Fourier transform for PVC and the nanocomposites. Several parametric values can be identified and given in Table 1: (a) maximum force F_{max}; (b) energy absorbed up to maximum force, defined as the initiation energy E_{init}; (c) propagation energy E_{prop}; (d) total fracture energy E_T; (e) load rise time up to peak force, t_r; (f) initiation time, t_{init}; and (g) propagation time, t_{prop}. It is apparent that F_{max}, E_{init}, E_{prop}, E_T, t_r and t_{init} increase with nano-Sb_2O_3 particles loading to 2.5 wt% and then decreases at larger loadings. These observations agree with the tensile and impact properties. Thus, we believe the nano-Sb_2O_3 particles prolong the crack initiation time due to the strong interaction between the nanoparticles and PVC matrix enhanced by the PMMA shell coated on the particle surface, and increase the energies for crack initiation and impact fracture. All these events will toughen the nanocomposites.

The role of inorganic rigid particles in toughening polymer composites is similar to cavitation of soft rubber particles in polymer blends. Ramsteiner and Heckmann [50] have shown that stress whitening in rubber-toughened blends is attributed to the cavitation of rubber particles. As mentioned earlier, stress-whitening occurred when

Table 1
Drop-weight dart impact fracture parameters of PVC–Sb_2O_3 nanocomposites

Samples	Sb_2O_3 (%)	F_{max} (N)	E_T (J)	t_r (ms)	t_{init} (ms)	E_{init} (J)	t_{prop} (ms)	E_{prop} (J)
PVC-1	0	291.73	0.15	0.699	0.503	0.10	0.196	0.05
PVC-2	2.5	470.11	0.27	0.728	0.542	0.18	0.186	0.09
PVC-3	5	410.00	0.19	0.596	0.422	0.12	0.174	0.07
PVC-4	7.5	378.77	0.17	0.600	0.419	0.11	0.181	0.06

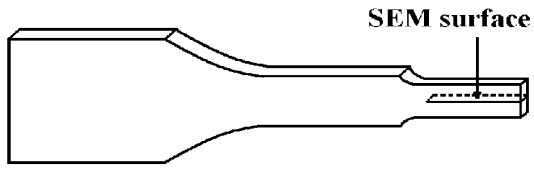

Fig. 15. Schematic illustration of necked down region for SEM examination.

PVC/Sb_2O_3 nanocomposites were stretched. To evaluate the toughening mechanisms in these nanocomposites, we obtained a longitudinal cryo-fractured surface of the necked down region at mid-thickness, Fig. 15, of a tensile specimen and examined the failure morphology with SEM as shown in Fig. 16. For the pure PVC, it can be seen from Fig. 16(a) that there are many cavities leading to semi-brittle failure. For PVC/Sb_2O_3 nanocomposites, the PVC matrix was severely deformed and drawn around the particles, Fig. 16(b)–(d). In the necked region, there were triaxial stresses, which were locally elevated at the particles acting as stress concentrators leading to debonding at the nanoparticle-polymer interface. With increased loading, the debonded interfaces would deform forming ellipsoidal voids as the ligaments between them were further drawn or stretched longitudinally. The PMMA shell covered on the surface of the nano-Sb_2O_3 particles increases the interaction of the nanoparticles with PVC matrix and enhances their dispersion in the PVC matrix. This promotes a more homogeneous debonding/voiding and matrix drawing mechanism, which absorbs more energy and toughens the PVC. If the loading of the nano-Sb_2O_3 particles is large, Figs. 16(c) and (d), then some nanoparticles agglomerate weakening the interfacial adhesion, reducing the number of debonding/voiding sites and hence decreasing the toughness of the nano-composites as may be approximately and qualitatively represented by the areas under the tensile stress–displacement curves in Fig. 8.

4. Conclusions

Based on the outcomes and results obtained in this study, we can draw some definitive conclusions. Nano-sized Sb_2O_3 particles do not inhibit polymerization of MMA during in-situ MMA/Sb_2O_3 polymerization. The PMMA shell covered on the surface of nano-Sb_2O_3 particles increases the interaction between the nanoparticles and PVC matrix, which leads to the breakdown of nano-Sb_2O_3 particle agglomerates, enhances nano-Sb_2O_3 particles dispersion in PVC, and improves interfacial adhesion between particle and matrix. It is shown that nano-Sb_2O_3 particles stiffen, strengthen and toughen PVC matrix with the maximum effect at 2.5 wt% of nano-Sb_2O_3 particles. Examination of the tensile fractured samples indicates that debonding/voiding at the particle-matrix interface and inter-particle

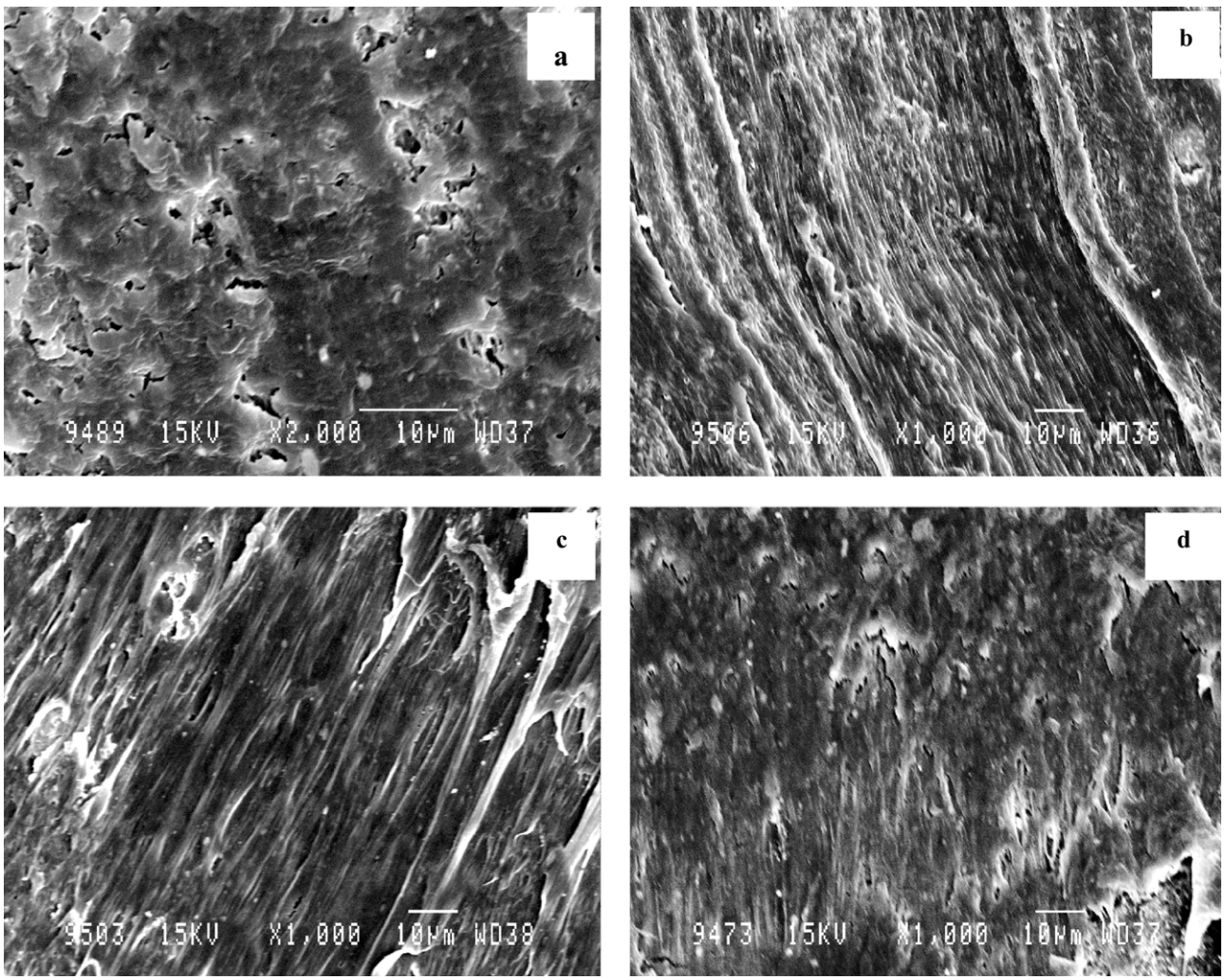

Fig. 16. SEM micrographs showing the longitudinally cryogenic-fractured necked region of PVC and PVC/Sb_2O_3 nanocomposites. (a) Pure PVC; (b) 2.5 wt% nano-Sb_2O_3; (c) 5.0 wt% nano-Sb_2O_3; and (d) 7.5 wt% nano-Sb_2O_3.

ligament drawing account for the large energy absorption of the nanocomposites. In impact fracture, the nano-Sb_2O_3 particles prolong crack initiation time and increase the energies for crack initiation and crack propagation due to the strong interfacial interaction between the nanoparticles and the PVC matrix. All these toughening mechanisms in tensile and impact tests become less effective when the nanoparticles start to agglomerate.

Acknowledgements

The authors are grateful for the financial support of the National Natural Science Foundation of China (50003005 and 10172037) and the Australian Research Council (ARC) for their continuing support of the project on 'Polymer Nanocomposites'. YWM wishes to acknowledge the award of an Australian Federation Fellowship by the ARC tenable at the University of Sydney. XLX is Visiting Scholar to the CAMT supported by the ARC.

References

[1] Yano K, Usuki A, Yurauchi T, Kamigaito O. J Polym Sci, Part A: Polym Chem 1993;31:2493.
[2] Godovski DY. Adv Polym Sci 1995;119:79.
[3] Giannelius EP. Adv Mater 1996;8:29.
[4] Kurokawa Y, Yasudo H, Kashiwagi M, Oyo A. J Mater Sci Lett 1997; 16:1670.
[5] Kawasumi M, Hasegawa N, Kato M, Usuki A, Okada A. Macromolecules 1997;30:6333.
[6] Kim GM, Lee DH, Hoffmann B, Krressler J, Stöppelmann G. Polymer 2000;42:1095.
[7] Gilman JW, Jackson CL, Morgan AB, Harris R, Manias E, Giannelis EP, Wuthenow M, Hilton D, Phillips SH. Chem Mater 2000;12:1866.
[8] Cho JW, Paul DR. Polymer 2001;42:1083.
[9] Chan CM, Wu JS, Li JX, Cheung YK. Polymer 2002;43:2981.
[10] Ou YC, Yang F, Yu ZZ. J Polym Sci, Part B: Polym Phys 1998;36: 789.

[11] Yang F, Ou YC, Yu ZZ. J Appl Polym Sci 1998;69:355.
[12] Levita G, Marchetti A, Lazzeri A. Polym Engng Sci 1989;19:39.
[13] Petrovicova R, Knight R, Schadler LS, Twadowski TE. J Appl Polym Sci 2000;78:2272.
[14] Petrovic ZS, Javni I, Waddon A, Banhegi G. J Appl Polym Sci 2000; 76:133.
[15] Rong MZ, Zhang MQ, Zheng YX, Walter R, Friedrich K. Polymer 2001;42:167.
[16] Rong MZ, Zhang MQ, Zheng YX, Friedrich K. Polymer 2001;42: 3301.
[17] Kickelbick G. Prog Polym Sci 2003;28:83.
[18] Saujanya C, Radhakrishnan S. Polymer 2001;42:6723.
[19] Zuiderduin WCJ, Westzaan C, Huétink J, Gaymans RJ. Polymer 2003;44:261.
[20] Huang HH, Orler B, Wilkes GL. Polym Bull 1985;14:557.
[21] Ellsworth MW, Novak BM. J Am Chem 1991;113:2756.
[22] Coltrain BK, Ferrar WT, Landry CJT, Molaire TR, Zumbulyadis N. Chem Mater 1992;4:358.
[23] Landry CJT, Coltrain BK, Teegarden DM, Long TE, Long VK. Macromolecules 1996;29:4712.
[24] Breiner JM, Mark JE. Polymer 1998;39:5483.
[25] Kiss G. Polym Engng Sci 1987;27:410.
[26] Krishnamoorti R, Vaia RA. Polymer nanocomposites. Washington, DC: American Chemical Society; 2001.
[27] Hergeth WD, Peller M, Hauptmann P. Acta Polym 1986;37:468.
[28] Hergeth WD, Starre P, Schmutzer K. Polymer 1988;29:1323.
[29] Hergeth WD, Steinau UJ, Bittrich HJ, Simon G, Schmutzer K. Polymer 1989;30:254.
[30] Bourgeat-Lami E, Espiard P, Guyot A, Briat S, Gauthier C, Vigier G, Perez J. ACS Symp Ser 1995;585:112.
[31] Bourgeat-Lami E, Espiard P, Guyot A. Polymer 1995;36:4385.
[32] Bourgeat-Lami E, Espiard P, Guyot A, Gauthier C, David L, Vigier G. Angew Makromol Chem 1996;242:105.
[33] Bourgeat-Lami E, Lang J. J Colloid Interface Sci 1998;197:293.
[34] Bourgeat-Lami E, Lang J. J Colloid Interface Sci 1999;210:281.
[35] Bourgeat-Lami E, Lang J. Macromol Symp 2000;151:337.
[36] Xie XL, Li BG, Pan ZR, Li RKY, Tjong SC. J Appl Polym Sci 2001; 80:2105.
[37] Tang CY, Xie XL, Zhou XP, Jia XH, Li RKY. J Mater Sci Lett 2002; 21:815.
[38] Mills NJ, Zhang PS. J Mater Sci 1989;24:2099.
[39] Aggag G, Takahashi K. Polym Engng Sci 1996;36:2260.
[40] Tjong SC, Li RKY, Xie XL. J Appl Polym Sci 2000;77:1964.
[41] Xie XL, Li RKY, Mai Y-W. Polym Engng Sci 2002;42:452.
[42] Xie XL, Fung KL, Li RKY, Tjong SC, Mai Y-W. J Polym Sci, Part A: Polym Phys 2002;40:1214.
[43] Sumita M, Shizuma T, Miyasaka K, Ishikawa K. J Macromol Sci Phys 1983;B22:601.
[44] Sumita M, Tsukrmo T, Miyasaka K, Ishikawa K. J Mater Sci 1983;18: 1758.
[45] Olabisi O, Robeson LM, Shaw MT, Polymer–polymer miscibility, New York: Academic Press; 1979.
[46] Guth E. J Appl Phys 1945;16:20.
[47] Nicolais L, Narkis M. Polym Engng Sci 1971;11:194.
[48] Turcsányi B, Pukánszky B, Tüdös F. J Mater Sci Lett 1988;7:160.
[49] Dekkers MJE, Heikens D. J Appl Polym Sci 1985;30:2389.
[50] Ramsteiner F, Heckmann W. Polym Commun 1985;26:199.